Total internal reflection ellipsometry for kinetics-based assessment of bovine serum albumin immobilization on ZnO nanowires

Ieva Plikusiene, Vincentas Maciulis, Octavio Graniel, Mikhael Bechelany, Saulius Balevicius, Vilius Vertelis, Zigmas Balevicius, Anton Popov, Arunas Ramanavicius, Almira Ramanaviciene

Total internal reflection ellipsometry for kinetics-based assessment of bovine serum albumin immobilization on ZnO nanowires

Ieva Plikusiene[a,b], Vincentas Maciulis[b], Octavio Graniel[c], Mikhael Bechelany[c], Saulius Balevicius[b], Vilius Vertelis[b,d], Zigmas Balevicius[b], Anton Popov[a], Arunas Ramanavicius[a,b] Almira Ramanaviciene[a]*

[a] NanoTechnas – Center of Nanotechnology and Materials Science, Faculty of Chemistry and Geosciences, Vilnius University, Naugarduko str. 24, 03225 Vilnius, Lithuania

[b] State Research Institute Center for Physical and Technological Sciences, Sauletekio ave. 3, Vilnius, Lithuania

[c] Institut Europeen des Membranes, IEM, UMR-5635, Universite de Montpellier, ENSCM, CNRS, Place Eugene Bataillon, 34095 Montpellier Cedex 5, France

[d] French-German Research Institute of Saint-Louis, Saint-Louis, 68300, France

*Corresponding author:

Prof. dr. Almira Ramanaviciene; e-mail: almira.ramanaviciene@chf.vu.lt;

Abstract

The ZnO material exhibits a rich family of nanostructures, which show great potential for the sensitivity improvement of optical detection systems. In this work, ~350 nm ZnO nanowires (ZnO-NWs) were electrochemically deposited on ZnO and indium tin oxide coated glass (ZnO-NWs/ZnO/ITO/glass) substrate. ZnO-NWs were modified with *N*-(3-Aminopropyl)triethoxysilane (APTES) for covalent bovine serum albumin (BSA) immobilization. The studies were performed using spectroscopic total internal reflection ellipsometry (TIRE) setup based on the Kretschmann configuration. The refractive index dispersion of ZnO-NWs in the air was obtained from the optical model applying Bruggeman effective medium approach. It was determined that ZnO-NWs effective layer consists of 30 % ZnO and 70 % void. Reflectance difference before and after ZnO-NWs modification with BSA was 6.6 times higher than in the case of plain ZnO layer. The Δ kinetics of covalent BSA immobilization on APTES/ZnO-NWs/ZnO/glass substrate contains two phases. Evaluation of diffusion coefficient for BSA into PBS filled APTES/ZnO-NWs/ZnO/ITO/glass was performed using numerical calculation, and the obtained diffusion coefficient was $2.4 \cdot 10^{-17}$ m^2/s. Simulation of BSA immobilization on flat ZnO layer and on ZnO-NWs modified surface showed that 13 times higher sensitivity for wavelength to refractive index change was observed for the substrate with ZnO-NWs.

Keywords: total internal reflection ellipsometry; zinc oxide nanowires; covalent bovine serum albumin binding kinetics; diffusion coefficient.

1. Introduction

Recently, metal oxides have been applied to different analytical systems thanks to their facile preparation and their non-toxicity [1]. Zinc oxide (ZnO) is an n-type semiconductor with wide band gap (3.37 eV) and a large exciton binding energy (60 meV), and high isoelectric point (pH 9.0–9.5). It is non-toxic, biocompatible and owns a number of specific advanced features such as thermal stability, enhanced electron mobility, high mechanical strength and environmental stability for oxidation [2]. ZnO and various nanostructures formed from this metal oxide attract a high interest for their application in transparent electronics, photocatalysis, solar cells, supercapacitors, sensors and optical biosensors [3,4,5,6,7,8,9]. ZnO nanowires (ZnO-NWs) are typical 1D ZnO nanostructures and due to their large surface area, direct electron pathway in the c-axis direction, good biocompatibility and chemical stability were used in the development of nano-size electrodes [10,11]. The surface of ZnO-NWs is relevant for functionalization providing an effective immobilization of biomolecules with appropriate loading capacity, high biological activity and good stability [12].The diameters of ZnO nanostructures are close to the sizes of the biological and chemical molecules that why such 1D nanostructures can be excellent transducers.

Nowadays optical analytical systems play an important role in the detection of a wide range of biological and chemical substances. The main advantages of the optical sensing include non-destructive nature of analytical signal registration, real-time, label-free or label-based detection of analyte with a high sensitivity, selectivity and reliability, and in cost effective manner. Optical biosensors based on measurements of absorbance, reflectance, photoluminescence, scattering, polarisation or refractive index of the biological medium are the next generation of sensing devices for everyday use [13,14,15,16]. The value of optical response (which is related to sensitivity) strongly depends on amount of biomaterial immobilized on the sensor surface. In order to increase the sensitivity, it is necessary to accrue an optimal surface density of biomolecules and proper orientation on the surface of the sensor. This can be realized using nanostructures, such as nanowires grown on the substrate, which increase the effective surface area of the sensor. However, the nanowires usually exhibit strong diffuse scattering effect, which aggravate the optical signal registration due to very low specular reflectance intensity [17,18]. This effect would be the drawback if conventional optical measurements like absorbance, reflectance or transmittance are used. In such case the ellipsometry method, which measure relative values of *p*- and *s*-polarized light amplitude ratio Ψ and the phase differences Δ between them is less influenced by a weak reflectance intensity. Unfortunately, this advantage of conventional ellipsometry method is weakened by light depolarization effect appearing in case of highly diffuse scattered surfaces [19]. For this reason, better solution would be application of spectroscopic

ellipsometry combined with surface plasmon resonance method, which usually is used for real-time monitoring of proteins interactions at solid-liquid interface, that is called total internal reflection ellipsometry (TIRE) [20,21,22]. The TIRE configuration minimize the depolarization effect because light do not pass directly through the highly scattered surface, but entered in to the structure of nanowires as a evanescent surface wave generated due to total internal reflection phenomenon [13]. It was shown that higher sensitivity of this method in case of multilayered ZnO structures have been achieved because of multiple reflections of the light occurring in a total internal reflection mode. Especially it was noticeable for ellipsometric parameter Δ, which under total internal reflection condition depends on the angle of incidence [23,24,25].

The aim of this study has been to investigate properties of ZnO-NWs surface by utilizing spectroscopic ellipsometry under TIRE configuration during covalent BSA immobilization on ZnO-NWs. The capabilities of surface structures containing ZnO-NWs for the optical signal enhancement under total internal reflection mode and real-time measurement of covalent BSA binding were discussed from the sensitivity point of view. Additionally, evaluation of diffusion coefficient based on one dimensional diffusion equation was performed.

2. Materials and methods

2.1 Materials

N-(3-Aminopropyl)triethoxysilane (APTES, 99%) and 1-(ethyl-3-(3-diaminopropyl)carbodiimide)hydrochloride (EDC) were obtained from Sigma-Aldrich (Germany). *N*-Hydroxysuccinimide (NHS) was obtained from Merck (Germany). Diethylzinc, $ZnCl_2$ (CAS: 7646-85-7, purity > 98%) and potassium chloride (KCl, CAS: 7447-40-7, purity > 99%) were purchased from Fluka (Germany). Bovine serum albumin (BSA, fraction V) was obtained from Carl Roth GmbH & Co (Karlsruhe, Germany). Phosphate buffered saline (PBS) tablets (0.14 M NaCl, 0.0027 M KCl, 0.01 M phosphate buffer pH 7.4) were purchased from AB Medicago (Sweden). All chemicals were of analytical grade or better. All aqueous solutions were prepared in UHQ water (conductivity less than 1 $\mu S\ cm^{-1}$) and purified by DEMIWA rosa 5 (WATEK, Czech Republic). Glass plates covered with a 120 nm ITO layer were obtained from Kintec (Hong Kong).

2.2 Preparation of ZnO-NWs

The ZnO-NWs were prepared as follows. Firstly, a 20 nm ZnO layer was deposited on the ITO/glass substrates ($1 \times 2\ cm^2$) by atomic layer deposition method in a home-made system with diethylzinc (DEZ) and deionized water as precursors [26,27]. The deposition of ZnO was achieved by exposing the ITO/glass substrates to sequential pulses of DEZ and deionized water separated by a purge of argon at

a constant temperature of 100 °C. A typical cycle consisted of a 0.2 s pulse of DEZ, 40 s exposure, and a 60 s purge with argon, followed by a 2 s pulse of deionized water, 40 s exposure, and a 60 s purge with argon. Afterward, ZnO-NWs were grown on the ZnO/ITO/glass substrate by electrodeposition in a three electrode configuration following a previously reported procedure [23]. Briefly, a solution of 0.05 mM of $ZnCl_2$ (zinc precursor) and 0.1 M of KCl (supporting electrolyte) was prepared and used as electrolyte with the ZnO/ITO/glass as the working electrode, a Pt plate as the counter electrode, and Ag/AgCl as the reference electrode. The electrodeposition was performed at 80 °C with a constant electric potential of −1.0 V for 30 min in a VersaSTAT 3 potentiostat, while O_2 was constantly bubbled in the electrolyte solution. Once the electrodeposition was completed, the ZnO-NWs/ZnO/ITO/glass substrates were thoroughly rinsed with deionized water.

2.3 Silanization of ZnO-NWs/ZnO/ITO/glass substrates by APTES

Silane-derivation of ZnO-NW deposited on ZnO/ITO/glass substrates was performed by a vapor-phase deposition process according to the procedure described earlier [24].To minimize the influence of humidity, silanization was performed in a glovebox in an inert atmosphere. A few drops of APTES were deposited in a small vial, which was then placed next to the sample located in a glass Petri dish. The heat resistant insulation tape was used for the covering of Petri dish and isolation of surface from the contact with air. The covered Petri dish was then placed in an oven and kept overnight at 90 °C. Afterwards, the APTES modified ZnO-NWs were washed with toluene, ethanol and distilled water and then dried in an oven at 110 °C. In this way, the surface of ZnO-NWs was functionalized with amino groups (APTES/ZnO-NWs/ZnO/ITO/glass), which are necessary for covalent immobilization of BSA.

2.4 Covalent immobilization of BSA on APTES/ZnO-NWs/ZnO/ITO/glass surface

In order to immobilize BSA covalently on the salinized surfaces of the ZnO-NWs, the carboxyl groups present in BSA were activated for 15 min by a mixture of EDC and NHS aqueous solutions. In details, 1.0 mg/ml concentration solution of BSA in PBS was mixed with EDC and NHS, and the final concentrations of EDC, NHS and BSA were 400 mM, 100 mM and 0.1 mg/ml, respectively. The activated carboxyl groups of BSA were exposed to the amino groups present on APTES/ZnO-NWs/ZnO/ITO/glass surface.

2.5 TIRE measurements

The ellipsometric experiments were conducted using a rotating compensator based ellipsometer J. A. Woollam M2000X (Lincoln, USA). The TIRE experiments were carried out at a 70° angle of incidence with the illumination being at wavelengths in the 210–1000 nm spectral range. This was conducted using a BK7 glass 70° angle prism connected *via* a refractive index matching fluid with the

ZnO-NWs/ZnO/ITO/glass substrate. In the TIRE experiment, a liquid handling system with a custom-built teflon chamber was used. In this chamber the sensing surfaces were placed. The connecting valve was then opened, allowing the PBS to be injected into the chamber, which was needed for the performance of covalent BSA immobilization on the modified surface. TIRE measurement before and after ZnO-NWs covalent modification with BSA were performed and registered signals were compared.

3. Results and discussion

3.1 Characterization of ZnO-NWs by SEM

ZnO-NWs were successfully formed on 20 nm ZnO layer by electrodeposition method. The cross-section view of ZnO-NWs array on ZnO/ITO/glass substrate obtained by scanning electron microscopy (SEM) is presented in figure 1. As it can be seen from this figure the ZnO-NWs mainly consist of ≈ 40 nm width and ≈ 350 nm length wires oriented at two angles (≈ 60º and 120º) to the substrate plane.

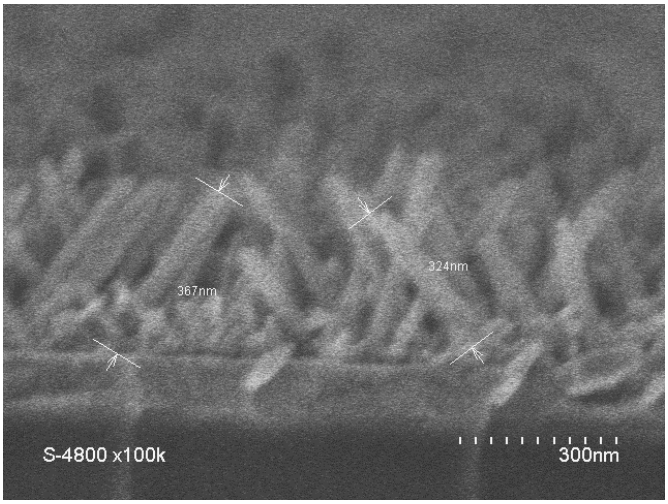

Fig. 1. SEM imagine of ZnO-NWs deposited on ZnO/ITO/glass substrate.

Also it has to be noted that the density of the nanowires slightly fluctuated at different places of the substrate. The fluctuations of the density are related to different angles orientation and unequal distance between nanowires. As it can be seen from figure 1 in some parts of formed surface nanowires are crowded or unevenly distributed. For estimation of the ratio (fill factor $f = V_{NW}/V_t$) between volume occupied by ZnO-NWs (V_{NW}) and total space of ZnO-NWs cover (V_t), we calculate the linear density of ZnO-NWs ($\rho_l = l_{NW}/l_t$) using the cut plane of SEM picture presented in figure1. Here l_{NW} is sum of diameters (D_{NW}) of ZnO-NWs displaced near the cut plane and l_t is the total length of this cut. It was found that $\rho_l \approx 0.536$. Assuming that cross section of single ZnO-NWs is D_{NW}^2 and taking into consideration that $f = V_{NW}/V_t = S_{NW}/S_t$, here S_{NW} is square occupied by ZnO-NWs and S_t is total cover

area, the fill factor in percentages can be obtained by simple formula $f = \rho_f^2 \times 100\%$. Thus in our case the $f \approx 28.7$ %. This value corresponds to ZnO-NWs occupied volume.

3.2 Optical properties of ZnO-NWs deposited on ZnO/ITO/glass substrate

In order to analyze contribution of ZnO-NWs to the optical response, the simulation of multilayer system with plain ZnO layer was conducted. This simulation has been done in TIRE configuration for reflectance intensity and ellipsometric parameters for the structures: 1 – ZnO/ITO/glass, 2 – APTES/ZnO/ITO/glass, and 3 – BSA/APTES/ZnO/ITO/glass. Simulated data are shown in figure 2A. For structure APTES/ZnO/ITO/glass the difference from ZnO/ITO/glass was negligible, for this reason it is not showed here.

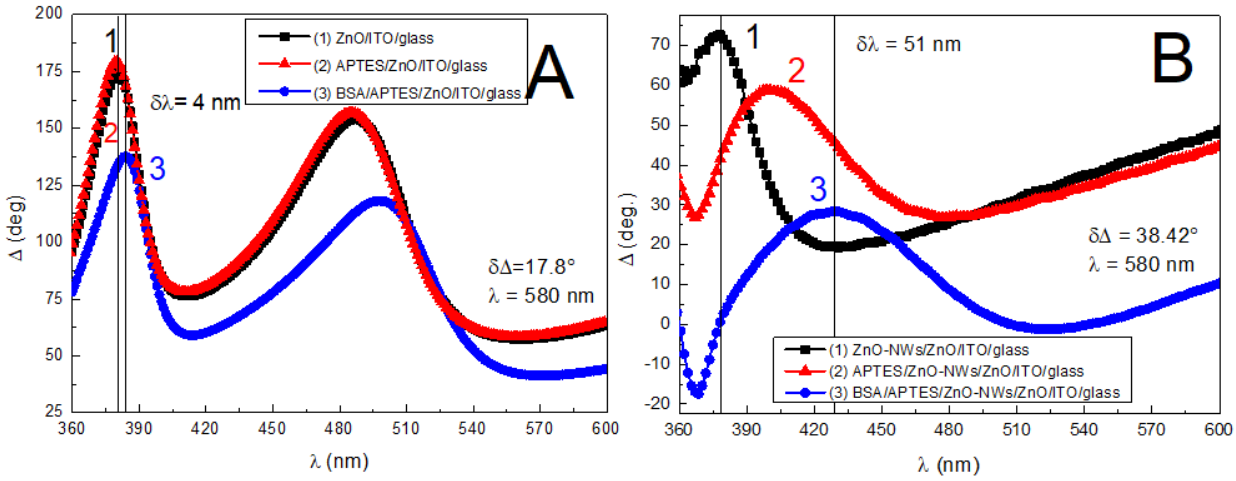

Fig.2. Simulation of ellipsometric parameter *Δ vs* wavelength during flat ZnO modification. A) experimental curves of ellipsometric parameter *Δ vs* wavelength for 1–ZnO/ITO/glass, 2–APTES/ZnO/ITO/glass; 3–BSA/APTES/ZnO/ITO/glass B) experimental curves of ellipsometric parameter *Δ vs* wavelength for 1–ZnO-NWs/ZnO/ITO/glass, 2–APTES/ZnO-NWs/ZnO/ITO/glass and 3–BSA/APTES/ZnO-NWs/ZnO/ITO/glass.

The experimentally obtained results for ellipsometric parameter *Δ* dependence on the wavelength λ for 1 – ZnO-NWs/ZnO/ITO/glass, 2 – APTES/ZnO-NWs/ZnO/ITO/glass, and 3 – BSA/APTES/ZnO-NWs/ZnO/ITO/glass are presented in figure 2B. Here we present only spectra for ellipsometric parameter *Δ* as it was proofed to have higher sensitivity [25]. In case of non-modified structure ZnO-NWs/ZnO/ITO/glass ellipsometric parameter *Δ* (λ) peak was observed at 377 nm, such structure effective refractive index was estimated to be $n_{ZnO\text{-}NWs}$=1.355 at 580 nm, using effective medium approximation (EMA). Meanwhile, after ZnO-NWs modification with APTES,

which effective refractive index was modeled to be $n_{APTES} = 1.521$ at 580 nm Δ (λ) peak was redshifted to 401 nm value. As it can be seen from figure 2B, redshift observed between two curves before modification of ZnO-NWs (Fig. 2, curve 1) and after modification of ZnO-NWs by APTES (Fig. 2, curve 2) was equal to 23 nm when difference between refractive indexes was n_{APTES}-$n_{ZnO\text{-}NWs} = 0.166$. After further covalent immobilization of BSA on APTES/ZnO-NWs/ZnO/ITO/glass redshift ellipsometric parameter Δ for 28 nm was registered, refractive index of such structure (BSA/APTES/ZnO-NWs/ZnO/ITO/glass) was n_{BSA}=1.691 (at 580 nm). Calculated difference was n_{BSA}- $n_{APTES} = 0.17$. The total change in refractive index before and after modification of ZnO-NWs/ZnO/ITO/glass using BSA was n_{BSA}-$n_{ZnO\text{-}NWs} = 0.366$ and total shift between peaks of 1–ZnO-NWs/ZnO/ITO/glass and 3–BSA/APTES/ZnO-NWs/ZnO/ITO/glass was 51 nm. Calculated sensitivity of structure BSA/APTES/ZnO-NWs/ZnO/ITO/glass was 151.8 nm/RIU.

In case of flat-type ZnO structure (ZnO/ITO/glass) simulation before and after modification by APTES and BSA (Fig. 2A curves 1, 2, 3) the observed redshift was only 4 nm when difference between refractive indexes was n_{BSA}-$n_{ZnO} = 0.366$. The clear difference before and after modification of ZnO/ITO/glass with APTES was not observed, the curves 1 and 2 in figure 2A overlaps each other. The simulated difference between refractive indexes n_{BSA}-n_{ZnO} for structures ZnO/ITO/glass and BSA/APTES/ZnO/ITO/glass was used the same as calculated between ZnO-NWs/ZnO/ITO/glass and 3–BSA/APTES/ZnO-NWs/ZnO/ITO/glass. The sensitivity of such structure was estimated to be 11.9 nm/RIU. In case of ZnO-NWs as sensing substrate (ZnO-NWs/ZnO/ITO/glass) for covalent BSA immobilization, the sensitivity of spectral shift to refractive index was ~13 times higher in comparison to flat-type of ZnO.

The ellipsometric parameter Δ amplitude change at 580 nm in case of 350 nm flat-type ZnO/ITO/glass structure before and after modification with APTES and BSA (Fig. 2 A) was 17.8 degrees. Calculated sensitivity to refractive index change in this case was 53 degrees/RIU. For structures ZnO-NWs/ZnO/ITO/glass and BSA/APTES/ZnO-NWs/ZnO/ITO/glass (Fig. 2 B) Δ amplitude change at 580 nm was 38.42 degrees, calculated sensitivity was 114.3 degrees/RIU, ~2.24 times higher than in case of ZnO/ITO/glass and BSA/APTES/ZnO/ITO/glass. Such high sensitivity can be explained by the multiple reflections that occur into ZnO-NWs matrix when this structure is used as sensing layer in TIRE mode. Also these finding demonstrate that significantly higher amount of BSA molecules (or other proteins) can be covalently immobilized on ZnO-NWs modified substrate in comparison to flat-type ZnO layer due to higher surface area. These results allow us to suggest, that ZnO-NWs based optical analytical systems exhibit higher sensitivity and can be successfully used for the development of enzymatic and affinity biosensors.

Reflectance intensity (*R*) spectra presented in figure 3 show optical response for 1 – ZnO-NWs/ZnO/ITO/glass, 2 – APTES/ZnO-NWs/ZnO/ITO/glass, 2 – BSA/APTES/ZnO-NWs/ZnO/ITO/glass, 4 – ZnO/ITO/glass 5 – BSA/APTES/ZnO/ITO/glass. The reflectance of ZnO/ITO/glass before (Fig.3, curve 4) and after covalent immobilization of BSA (Fig.3, curve 5) values were between 0.8 and 1. These results show that almost all light was reflected in both cases and no clear difference between these curves was observed. Reflectance difference before and after modification of simulated flat ZnO/ITO/glass with APTES and BSA was only 0.021 a.u. at 650 nm. In case of flat-type ZnO/ITO/glass, BSA in PBS was modeled as infinite media using Cauchy dispersion which refractive index was 1.51 [24]. Structure BSA/APTES/ZnO-NWs/ZnO/ITO/glass BSA/APTES was modeled as effective media substrate, having 30% of ZnO and 70% Cauchy material, refractive index 1.691 at 580 nm.

It is reasonable to assume that ZnO-NWs contribute noticeable scattering effect from the surface, however simulation of optical response of the light scattered structure is rather complicated and limited due to software. Thus, the optical properties of ZnO-NWs formed on glass substrate covered with 120 nm ITO and 20 nm ZnO layers were measured by TIRE. Ellipsometric spectra were recorded using TIRE configuration at 70 degrees angle of incidence using 70 degrees BK7 glass prism for measurements in liquids. The reflectance intensity and ellipsometric spectra for ZnO-NW/ZnO/ITO/glass and BSA/APTES/ZnO-NWs/ZnO/ITO/glass presented in the figure 3. In contrary to the simulated structures with ZnO/ITO/glass, the ZnO-NWs had very weak reflectance intensity (Fig. 3, curve 1) due to strong light scattering effect, meanwhile ellipsometric spectra were less affected due to relative values of ellipsometric parameters. However, the differences in reflectance intensity spectra were clearly distinguished (Fig. 3, curves 1 and 3). In case of ZnO-NWs/ZnO/ITO/glass reflectance intensity values at 650 nm was observed to be 0.03 a.u., while after modification BSA/APTES/ZnO-NWs/ZnO/ITO/glass it became 0.17 a.u. Thus the *R* difference for the surface with ZnO-NWs before and after modification with BSA (Fig. 3, curves 1 and 3) was 0.14 a.u., and it was about 6.6 times higher in comparison to flat ZnO layer (Fig. 3, curves 4 and 5).

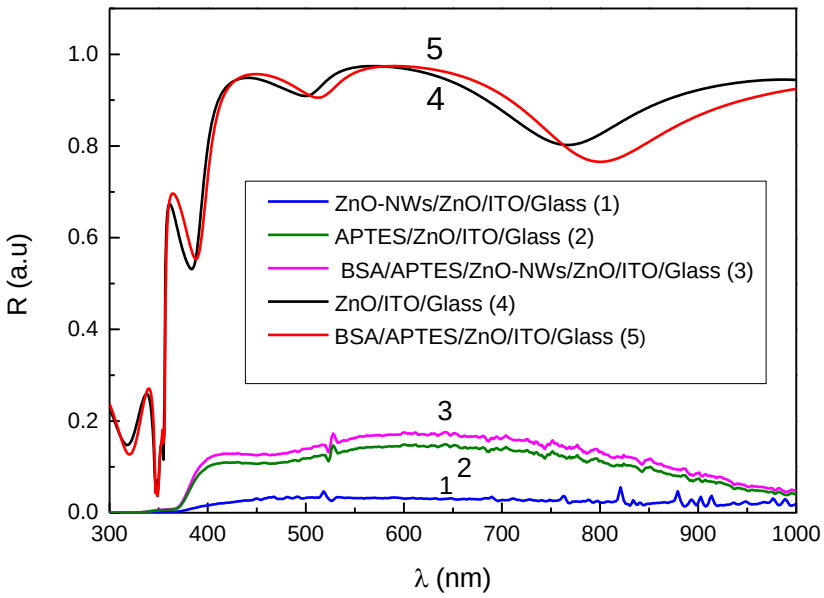

Fig. 3. Reflectance intensity (*R*) spectra of 1 – ZnO-NWs/ZnO/ITO/glass, 2 – APTES/ZnO-NWs/ZnO/ITO/glass, 3 – BSA/APTES/ZnO-NWs/ZnO/ITO/glass, 4 - ZnO/ITO/glass, 5 – BSA/APTES/ZnO/ITO/glass.

The differences of *R* spectra between ZnO/ITO/glass and ZnO-NWs/ZnO/ITO/glass after modification with APTES and covalent BSA immobilization can be explained by diminishing of diffuse scattering of ZnO-NWs due to BSA proteins binding. When such nanowires are modified with BSA, the surface structures become more "smooth" and as a result, the reflectance increase with higher refractive index of the layer. This phenomenon is observed as increased reflectance (Fig. 3, curve 3). However, such a low specular reflectance from the ZnO-NWs/ZnO/ITO/glass structure is rather complicated to reliably detect using *R* measurements. Meanwhile ellipsometry offer more stable optical detections at low intensity level due to relative value measurements through the ellipsometric prameters Ψ and Δ. Moreover, as noted above, the special behavior of ellipsometric parameter Δ increase sensitivity under conditions of total internal reflection because phase of *p*- and *s*-polarizations start to vary with angle of incidence. Such behaviour of ellipsometric parameter Δ is caused by difference of phase shifts between Fresnel reflection coefficients r_p and r_s for *p*- and *s*-polarizations, respectively [25].

In order to obtain ZnO-NWs matrix density, which has to be known for further presented diffusion evaluation, effective refractive index dependence on wavelength was modeled using Complete EASE software. Optical model for characterization of ZnO-NWs layer deposited on

ZnO/ITO/glass substrate was constructed using Bruggemen effective media approach in which the ZnO material layer was characterized using one PSemi-M0 and two Gaussian oscillators [26]. The effective ZnO-NWs layer thickness evaluated from SEM picture presented in figure 1 was ≈ 350 nm and it was fixed parameter during regression analysis. The obtained effective refractive index dispersion is presented in figure 4. Effective refractive index obtained from regression analysis showed that this ZnO-NWs layer consists of 30 % ZnO and 70 % void. Taking into consideration that average width of ZnO-NWs is ≈ 40 nm the width of void channels is from 40 to 90 nm.

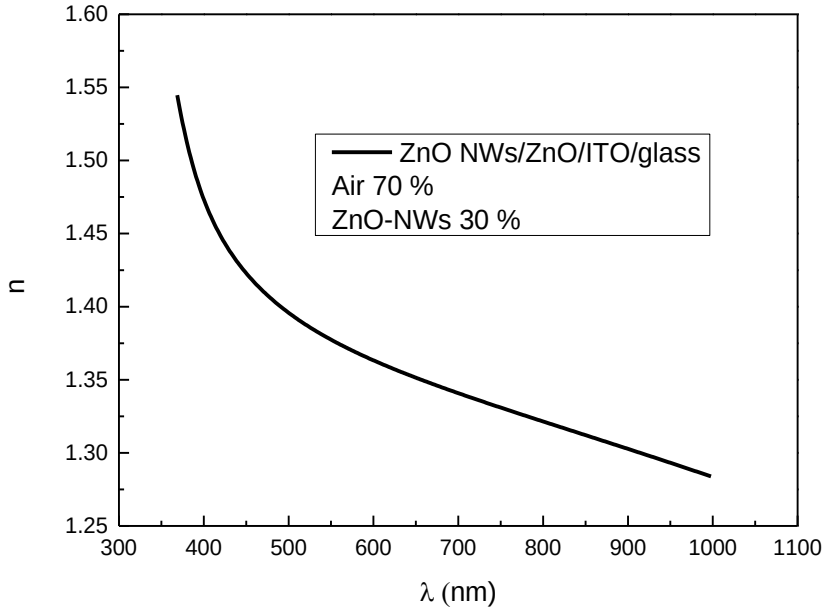

Fig. 4. Effective refractive index (n) *vs* wavelength (λ) obtained from optical model using Bruggeman effective media approach for structure ZnO-NWs/ZnO/ITO/glass in air.

Such evaluation of ZnO-NWs density which is obtained from modeling of ellipsometry measurements data is required for further analysis of BSA covalent immobilization in order to calculated diffusion coefficient. We used modeled values that corresponded to 30% of ZnO-NWs and 70% of air. This values coincides with that obtained from figure 1.

3.3 Kinetics of covalent BSA immobilization on APTES/ZnO-NWs/ZnO/ITO/glass substrate

The BSA immobilization kinetics was studied using 390.8 nm wavelength wave. The selection of this wavelength was made because at this point of spectra ellipsometric parameter Δ showed the highest sensitivity to refractive index changes.

For covalent BSA immobilization on APTES/ZnO-NWs/ZnO/ITO/glass substrate the surface was treated with PBS in order to establish the baseline. Figure 5 shows the variation of ellipsometric

parameter Δ during surface stabilization with PBS. The analysis of this variation had demonstrated that experimental curve can be well fitted by following formula:

$$\Delta(t) = \Delta_0 + \Delta_1 \cdot \exp(-t/t_1) + \Delta_2 \cdot \exp(-t/t_2); \quad (1)$$

Here t is time, Δ_0, Δ_1 and Δ_2 are constants. The characteristic times t_1 and t_2 are 4.5 min and 42 min, correspondingly. Shorter time t_1 most probably is related to a lower density regions of the nanowires matrix, meanwhile longer one corresponds to higher density regions.

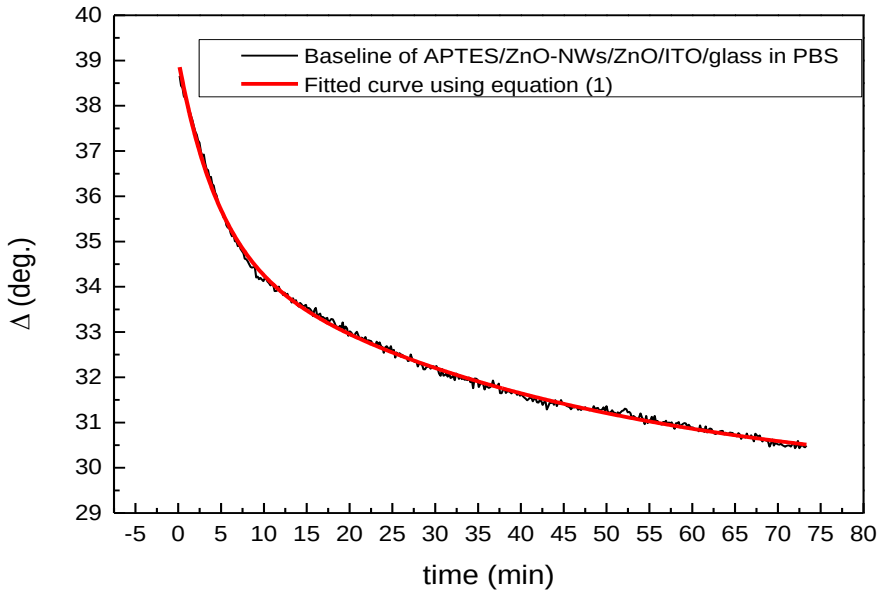

Fig. 5. Stabilization of APTES modified ZnO-NWs/ZnO/ITO/glass substrate in PBS and establishment of baseline.

After the establishment of steady state conditions and baseline in PBS, 0.1 mg/ ml concentration BSA solution in PBS was injected into the chamber with APTES/ZnO-NWs/ZnO/ITO/glass substrate. The Δ kinetics of covalent BSA immobilization on ZnO-NWs was recorded for 121 min. The kinetics of ellipsometric parameter Δ during the BSA immobilization process show changes of total ellipsometric parameter Δ about 6.11 degrees. As it can be seen from figure 6 the immobilization process after the steady state conditions in PBS were reached (PBS 1) contains two phases. The phase I of the kinetics takes place during relatively short time i.e. about 5 s and total change of Δ in this phase is only 0.5 degrees. An inset in fig.6 demonstrates the experimentally obtained BSA immobilization kinetics on flat-type ZnO structure (ZnO/ITO/glass). As it can be seen the amplitude and rise time of this process fully coincides with phase I showing that this phase is a result of BSA immobilization at the top of the ZnO-NWs. The ellipsometric parameter Δ change in flat-type ZnO

structure case is ~ 0.4 degree, meanwhile for ZnO-NWs (phase II) this change is about 5.2 degrees. Thus the ratio of these values showing the comparison of sensitivity between flat-type and ZnO-NWs platforms is about 13 times, that is in good agreement with simulations presented in section 3.2.

During the phase II the change of Δ was 5.61 degrees. Thus the biggest amount of injected BSA was covalently immobilized on APTES/ZnO-NWs/ZnO/ITO/glass substrate during the phase II of this process, which lasted more than 100 min. The average characteristic time of this phase, assuming that Δ parameter changing in time approximately can be described by exponential decay, was about 20 min. After covalent immobilization of BSA molecules on ZnO-NWs and washing with PBS, nonspecifically bounded molecules were removed from the surface. In this case total ellipsometric parameter Δ signal changed only by 0.17 degree, thus nonspecific adsorption of BSA on this surface was negligible (Fig. 6, PBS 2). It means that BSA was successfully covalently immobilized on the APTES/ZnO-NWs/ZnO/ITO/glass and layer of BSA is stable during the surface washing process.

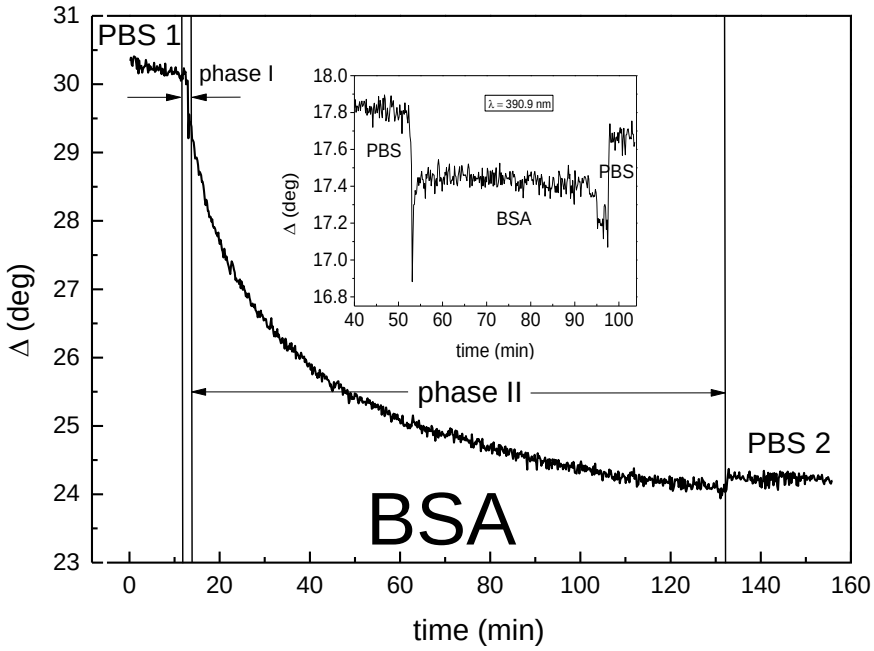

Fig. 6. Kinetics of BSA covalent immobilization on APTES/ZnO-NWs/ZnO/ITO/glass substrate.

Immobilization of BSA during the phase II demonstrates time-depending and irreversible bonding process. For this reason, we assumed that this phase appears due to BSA molecules diffusion in PBS solution through the narrow channels existing between nanowires (see Fig. 1). In order to verify this assumption, the following modelling of ellipsometric parameter Δ kinetics during BSA molecules immobilization was performed.

The ellipsometric parameter Δ_m measured using TIRE method is proportional to the effective refractive index (n_e) of the heterogenic matrix consisting of APTES/ZnO-NWs formed on ZnO/ITO/glass substrate and inter-wire space filled by PBS. During the diffusion of BSA molecules into this matrix filled by PBS, BSA changes its refractive index (n_{BSA}), which induces Δ_m value evolution in time. Using Maxwell Garnett approximation and assuming that Δ_m is directly proportional to the n_e it is possible to obtain following formula for Δ_m as a function of time (t):

$$\Delta_m(t) = \Delta_{ZnO}\left[\frac{2\delta(\Delta_{BSA}^2-\Delta_{ZnO}^2)+\Delta_{BSA}^2+2\Delta_{ZnO}^2}{2\Delta_{ZnO}^2+\Delta_{BSA}^2-\delta(\Delta_{BSA}^2-\Delta_{ZnO}^2)}\right]^{1/2}; \qquad (2)$$

Here Δ_{ZnO} and $\Delta_{BSA}(t)$ are ellipsometric parameters of APTES/ZnO-NWs and BSA solution in PBS corresondingly, δ is ratio of volumes between ZnO-NWs and inter wires space. The normalized measured ellipsometric parameter $\Delta_{nm} = [\Delta_m(t) - \Delta_m(0)]/[\Delta_m(\infty) - \Delta_m(0)]$ *vs* time dependence is presented in figure 7. Here: $\Delta_m(t)$, $\Delta_m(0)$ and $\Delta_m(\infty)$ are ellipsometric parameter Δ at different time instances, at the beginning, during phase I and at the phase II of BSA covalent immobilization .

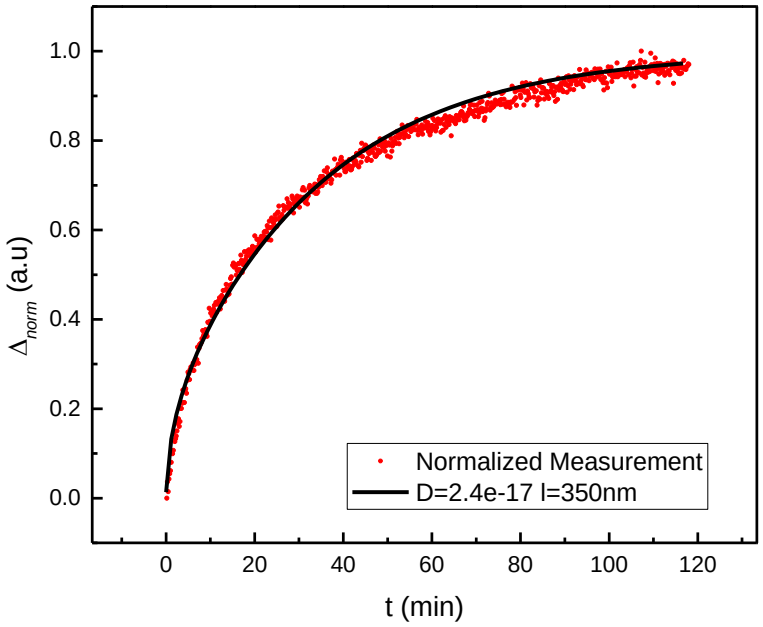

Fig.7. Dependence of the normalized signal Δ_{norm} of ellipsometric parameter *vs* time during BSA covalent immobilization on APTES/ZnO-NWs/ZnO/ITO/glass substrate.

Taking into consideration that optical properties, i.e. refractive index (n) of the solution, depends on concentration of BSA molecules, we assume direct proportionality between Δ_{BSA} and C. The distribution of this concentration in channel directed along nanowires as a function of time can be obtained by numerically solving a one dimensional diffusion equation:

$$D\frac{\partial^2 C(x,t)}{\partial x^2} = \frac{\partial C(x,t)}{\partial t}; \quad (3)$$

Here $C(x,t)$ is BSA molecules concentration, x is coordinate along nanowires, t is time and D is diffusion coefficient. The boundary conditions for this equation are following $C(0,0) = C(d,\infty) = C_0$ that is the concentration of BSA in PBS outside the nanowires matrix and $\partial C(d,t)/\partial t = 0$, here d is the length of channel filled only by PBS. The average concentration of BSA inside the channel (C_a) is:

$$C_a(t) = \frac{\int_0^d C(x,t)dx}{d}; \quad (4)$$

The results of numerical calculation of Δ_{norm} *vs* time dependence, obtained using (2), (3) and (4) equations show solid black curve presented in figure 8. For $\delta = 0.43$ (30 % ZnO and 70 % void) and $d = 350$ nm well-fitting of experimental data was at $D = 2.4 \cdot 10^{-17}$ m^2/s, that is about 6 orders lower than conventional BSA diffusion in PBS solution [28].Taking into consideration such low D value, BSA molecules dimension (14 nm × 4 nm × 4 nm) and diffusion channel width (40 – 90 nm) it is possible to assume that during covalent BSA immobilization on APTES/ZnO-NWs/ZnO/ITO/glass substrate BSA molecules diffusion plays a significant role. This process is not conventional Brownian diffusion, because during BSA molecules movement along the channel filled by PBS the interaction with ZnO-NWs is very important. For this reason, the value of diffusion coefficient has to be strongly correlated with the density of ZnO-NWs and dimensions of biomolecules. In this case the diffusion coefficient obtained from measurement and analysis of biomolecules immobilization kinetics could be used for the evaluation of these molecules size. Studies of D *vs* size dependence for various ZnO-NWs dimensions and surface densities would be an interesting object of further research.

4. Conclusions

It was demonstrated that ZnO-NWs produced by simple and cost-effective electrodeposition method on commercially available ITO/glass substrate coated with ZnO layer can be successfully applied for the BSA immobilization. This substrate is able to accumulate significantly higher amount of BSA molecules covalently immobilized on ZnO-NWs coated substrate in comparison to simulated flat-type ZnO layer. The TIRE method has shown that surfaces based on ZnO-NWs overtake the sensitivity of flat-type ZnO for wavelength to refractive index change by 13 times. Moreover, the surfaces with ZnO-NWs showed larger changes for ellipsometric parameters Ψ and Δ during the BSA binding to the ZnO-NWs surface. Particularly, changes of ellipsometric parameter Δ was 2.24 times more sensitive comparing to the flat-type ZnO sensor. TIRE method

allows to achieve higher sensitivity because Δ measured during BSA immobilization phase for ZnO-NWs was larger than that for the flat-type case. These differences in the phase were related to the distinct changes of refractive index of the ZnO-NWs and flat-type ZnO surfaces.

It was found that time of signal saturation in PBS buffer could be related to the different density of ZnO-NWs regions on the substrate. Shorter time of stabilization is related to lower density of ZnO-NWs, while longer time – to higher density of these nanostructures. The diffusion of proteins along the ZnO-NWs plays a significant role in this process, for this reason the diffusion coefficient is significantly lower than for proteins in free liquid space.

Declaration of competing interest

The authors declare that they have no known competing financial interests or personal relationships that could have appeared to influence the work reported in this paper.

Acknowledgments

This project has received funding from European Social Fund (project No 09.3.3-LMT-K-712-19-0106) under grant agreement with the Research Council of Lithuania (LMTLT).

References

[1] O. Graniel, M. Weber, S. Balme, P. Miele, M. Bechelany, *Biosens. Bioelectron.*, 2018, **122,** 147-159.
[2] A. Tereshchenko, M. Bechelany, R. Viter, V. Khranovskyy, V. Smyntyna, N. Starodub, R. Yakimova, *Sensor Actuat B-Chem.*, 2016, **229**, 664–677.
[3] D.-Y. Son, J.-H. Im, H.-S. Kim, N.-G. Park, *J. Phys. Chem*. C., 2014, **118**, 16567-16573.
[4] K.M. Lee, C.W. Lai, K.S. Ngai, J.C. Juan, *Water Res.*, 2016, **88**, 428-448.
[5] R. Viter, M. Savchuk, N. Starodub, Z. Balevicius, S. Tumenas, A. Ramanaviciene, D. Jevdokimovs, D. Erts, I. Iatsunskyi, A. Ramanavicius, *Sensor Actuat B-Chem.*, 2019, **285**, 601-606.
[6] G. Chai, O. Lupan, L. Chow, H. Heinrich, *Sensor Actuat A-Phys*, 2009, **150**, 184–187.
[7] M. Mehrabian, R. Azimirad, K. Mirabbaszadeh, H. Afarideh, M. Davoudian, *Physica E Low Dimens. Syst. Nanostruct.* 2011, **43**, 1141–1145.

[8] J.H. Jun, H. Seong, K. Cho, B. Moon, S. Kim, *Ceram. Int*., 2009, **35**, 2797–2801.
[9] A. Sanginario,V. Cauda, A. Bonanno, K. Bejtka, S. Sapienza, D. Demarchi, *RSC Adv*., 2016, **6**, 891.
[10] A. Kumar, S. Jung and T. Ji, *Sensors*, 2011, **11**, 5087-5111.
[11] A. Usman, O. Nur, M. Willander, B. Danielsson, *Sensor Actuat B-Chem*., 2010, **145**, 869–874.
[12] N. Tripathy and D-H Kim, *Nano Converg*., 2018, **5**, 27.
[13] C. Chen and J. Wang, *Analyst*, 2020, **145**, 1605-1628.
[14] X. Fan, I. M. White , S. I. Shopova, H. Zhu, J. D. Suter, S. Yuse, *Anal. Chim. Acta*., 2008, **620**, 8–26.
[15] A. Campu, L. Susu, F. Orzan, D. Maniu, A. M. Craciun, A. Vulpoi, L. Roiban, M. Focsan,. Astil. *Front. Chem.*, 2019, **7**, 55.
[16] P. Damborsky , J. Svitel, J. Katrlık, Essays Biochem., 2016, **60**, 91–100.
[17] J. Elias, C. l. Cle´ment, M. Bechelany, J. Michler, G. Y. Wang, Z. Wang, L. Philippe, *Adv. Mater.*, 2010, **22**, 1607–1612.
[18] J. Elias, M. Bechelany, I. Utke, R. Erni, D. Hosseini, J. Michler, L. Philippe, *Nano Energy.*, 2012, **1**, 696–705.
[19] M. Treideris, I. Simkiene, A.Selskis, Z. Balevicius, G.J. Babonas, *Acta Phys. Pol.*, 2011, **19**, 131-134.
[20] Z. Balevicius, J. Talbot, L. Tamosaitis, I. Plikusiene, A. Stirke, G. Mickiene, S. Balevicius, A. Paulauskas, A. Ramanavicius, *Sensor Actuat B-Chem*., 2019, **297**, 126770.
[21] I. Baleviciute, Z. Balevicius, A. Makaraviciute, A. Ramanaviciene, A. Ramanavicius, *Biosens. Bioelectron.*, 2013, **39**, 170-176.
[22] S. Zeng, D. Baillargeat, H. P. Ho, K. Yong, Chem. *Soc. Rev*., 2014, **43**, 3426-3452.
[23] O. Graniel, I. Iatsunskyi, E. Coy, C. Humbert, G. Barbillon, T. Michel, D. Maurin, S. Balme, P. Miele, M. Bechelany, *J. Mater. Chem. C*., 2019, **7**, 15066–15073.
[24] Z. Balevicius, A. Paulauskas, I. Plikusiene, L. Mikoliunaite, M. Bechelany, A. Popov, A. Ramanavicius, A. Ramanaviciene, *J. Mater. Chem. C*., 2018, **6**, 8778–8783.
[25] H. Arwin, M. Poksinski, K. Johansen, *Appl. Opt*., 2004, **43**, 15.
[26] A. A. Chaaya, R. Viter, I. Baleviciute, M. Bechelany, A. Ramanavicius, Z. Gertnere, D. Erts, V. Smyntyna, P. Miele, *J. Phys. Chem. C*., 2014, **118**, 3811-3819.
[27] M. Baitimirova, R. Viter, J. Andzane, A. Van Der Lee, D. Voiry, I. Iatsunskyi, E. Coy, L. Mikoliunaite, S. Tumenas, K. Zaleski, Z. Balevicius, I. Baleviciute, A. Ramanaviciene, A. Ramanavicius, S. Jurga, D. Erts, M. Bechelany, *J. Phys. Chem. C*., 2016, **120**, 23716–23725.
[28] S. Koutsopoulos, L. D. Unswortha, Y. Nagaia, S. Zhanga, *PNAS*, 2009, **106**, 4623–4628.